Solid-State 137Ba NMR Spectroscopy: An Experimental and Theoretical Investigation of 137Ba Electric Field Gradient Tensors and Their Relation to Structure and Symmetry

Hamaed, H.; Ye, E.; Udachin, K.; Schurko, R. W.

Publisher's version / Version de l'éditeur:
https://doi.org/10.1021/jp102026m
The Journal of Physical Chemistry B, 114, 18, pp. 6014-6022, 2010-04-21

Solid-State ^{137}Ba NMR Spectroscopy: An Experimental and Theoretical Investigation of ^{137}Ba Electric Field Gradient Tensors and Their Relation to Structure and Symmetry

Hiyam Hamaed,[†] Eric Ye,[‡] Konstantin Udachin,[§] and Robert W. Schurko*,[†]

Department of Chemistry and Biochemistry, University of Windsor, Windsor, Ontario, Canada N9B 3P4, Department of Chemistry, University of Ottawa, Ottawa, Ontario, Canada, K1N 6N5, and Steacie Institute for Molecular Sciences, National Research Council Canada, Ottawa, Ontario, Canada K1A 0R6

Received: March 5, 2010; Revised Manuscript Received: April 2, 2010

Ultrawideline ^{137}Ba SSNMR spectra of several barium-containing systems (barium nitrate, barium carbonate, barium chlorate monohydrate, barium chloride dihydrate, anhydrous barium chloride, and barium hydrogen phosphate) were acquired at two different magnetic field strengths (9.4 and 21.1 T) using frequency-stepped techniques. The recently reported WURST−QCPMG pulse sequence (O'Dell et al. *Chem. Phys. Lett.* **2008**, *464*, 97−102) is shown to be very useful for rapidly acquiring high signal-to-noise ^{137}Ba SSNMR spectra. The breadths of the second-order quadrupolar-dominated spectra and experimental times are notably reduced for experiments conducted at 21.1 T. Analytical simulations of the ^{137}Ba SSNMR spectra at both fields yield the quadrupolar parameters, and in select cases the barium chemical shift anisotropies (CSAs). Quadrupolar interactions dominate the ^{137}Ba powder patterns, with quadrupolar coupling constants, $C_Q(^{137}Ba)$, ranging from 7.0 to 28.8 MHz. The ^{137}Ba electric field gradient (EFG) parameters extracted from these spectra are correlated to the local environments at the barium sites, via consideration of molecular symmetry and structure, and first principles calculations of ^{137}Ba EFG tensors performed using CASTEP software. The rapidity with which ^{137}Ba SSNMR spectra can be acquired using the WURST pulse sequence and/or at ultrahigh magnetic fields and the sensitivity of the ^{137}Ba EFG tensor parameters to the changes in the barium environment suggest that ^{137}Ba SSNMR has great potential for structural characterization of a variety of barium-containing materials.

Introduction

The number of solid-state NMR (SSNMR) studies on quadrupolar nuclei continues to grow due to the development of new pulse sequences, improvements in NMR hardware, and the ever-increasing availability of NMR spectrometers with ultrahigh magnetic fields. There is burgeoning interest in the characterization of structure and dynamics at the molecular/atomic level from the perspective of quadrupolar nuclei, since they account for approximately 73% of the NMR-active nuclei in the periodic table, and are present in innumerable materials. Many quadrupolar nuclei are difficult to study by routine NMR methods, since they may have large quadrupolar interactions which result in immense spectral breadths, presenting challenges for both uniform excitation and detection, as well as acquisition of high signal-to-noise (S/N) NMR spectra. A variety of techniques have been developed for the rapid and efficient acquisition of quadrupolar-dominated powder patterns.[1−4] Recently, much work has been dedicated to the SSNMR spectroscopy of unreceptive quadrupolar nuclei (e.g., ^{79}Br, ^{127}I, ^{209}Bi, ^{115}In, ^{73}Ge, ^{14}N, ^{33}S, ^{87}Sr, ^{25}Mg, ^{43}Ca, etc.),[5−19] which are defined as nuclei which may have low gyromagnetic ratios, low natural abundances, broad anisotropic patterns, long relaxation times, or combinations of these characteristics. These studies have shown that such SSNMR spectra can provide rich structural information for a variety of materials; however, numerous challenges exist in acquiring broad powder patterns of high quality for inherently unreceptive nuclei.

Barium has two NMR-active isotopes, ^{137}Ba and ^{135}Ba, both of which are classified as unreceptive. Both have nuclear spins of 3/2, large nuclear electric quadrupole moments (Q = 24.5 and 16.0 fm^2, respectively),[20] small gyromagnetic ratios (2.9930 × 10^7 and 2.6755 × 10^7 rad T^{-1} s^{-1}, respectively), and low natural abundances (11.3 and 6.6%, respectively).[20] The combination of these properties renders the routine acquisition of barium NMR spectra very difficult. Despite the fact that ^{135}Ba has a smaller quadrupole moment, ^{137}Ba NMR is more commonly applied due to its higher receptivity (i.e., with respect to carbon, $D^C(^{137}Ba)$ = 4.62 and $D^C(^{135}Ba)$ = 1.93). In spite of the inherent difficulties encountered in ^{137}Ba NMR experiments, the resulting spectra can be very useful for probing the chemical environments of different barium sites, and a significant amount of information on structure and dynamics at the molecular level can be obtained. In particular, the quadrupolar interaction which is manifested in the central transition (+1/2 ↔ −1/2) of ^{137}Ba SSNMR spectra is very diagnostic. The quadrupolar interaction results from coupling of the nuclear quadrupole moment to the electric field gradient (EFG) at the nuclear origin. The EFGs are described by a symmetric, traceless, second-rank (3 × 3) tensor with three principal components defined such that $|V_{33}| \geq |V_{22}| \geq |V_{11}|$. The nuclear quadrupolar coupling constant, $C_Q = eQV_{33}/h$, and the asymmetry parameter, $\eta_Q = (V_{11} - V_{22})/V_{33}$, are sensitive to both major and minor structural changes, providing information on the spherical and axial symmetry, respectively, of the ground state electronic environments at the Ba sites.

^{137}Ba SSNMR experiments could increase our understanding of the numerous barium-containing systems important in dif-

* Author to whom correspondence should be addressed. Phone: (519) 253-3000, x3548. Fax: (519) 973-7098. E-mail: rschurko@uwindsor.ca.
[†] University of Windsor.
[‡] University of Ottawa.
[§] National Research Council Canada.

10.1021/jp102026m
Published on Web 04/21/2010

ferent applications such as glass manufacturing, well-drilling fluids, emulsification of liquids, NO storage, and the development of ultrasonic and electronic devices.[21−24] Notably, ^{137}Ba SSNMR may be especially valuable for characterization of materials for which crystal structures are unavailable or unobtainable (i.e., disordered solids, submicrocrystalline powders, etc.). However, of the relatively few ^{137}Ba SSNMR studies reported to date, most have focused on systems in which the barium sites exist in spherically symmetric environments, such as in BaO,[25] $BaTiO_3$,[25−28] $BaZrO_3$,[25] $YBa_2Cu_3O_y$,[29,30] and $Ba_xSr_{1-x}TiO_3$ ($0 \leq x \leq 1$),[31] which have small quadrupolar interactions and correspondingly narrow patterns.[25−27] MacKenzie et al. reported the ^{137}Ba NMR spectra of several barium-containing systems acquired under conditions of magic-angle spinning (MAS),[32] which were challenging to acquire due to the wide powder pattern breadths. Recently, Sutrisno et al. demonstrated the utility of $^{137/135}$Ba SSNMR experiments in probing the barium environment in β-barium borate.[33]

The problems associated with acquiring high S/N ^{137}Ba SSNMR spectra can be solved in part by the use of ultrahigh magnetic field strength spectrometers (i.e., 21.1 T) and/or the use of specialized SSNMR techniques such as the quadrupolar Carr−Purcell Meiboom−Gill (QCPMG) pulse sequence,[34] and the recently reported wideband uniform rate smooth truncation (WURST)−QCPMG sequence.[35−37] In addition, high S/N ultrawideline (UW) NMR spectra (i.e., ranging from 300 kHz to several MHz in breadth) can be rapidly acquired using stepwise (or piecewise) methods.[34,35,37−39] Individual subspectra with limited excitation bandwidths are acquired by stepping the transmitter frequency in even increments at a constant field strength, and then coadded or projected to obtain the total UWNMR pattern. The acquisition of such spectra can be very time-consuming, and this is further exacerbated for nuclei like ^{137}Ba, which has both a low natural abundance and low gyromagnetic ratio. However, the combination of the WURST−QCPMG pulse sequence and piecewise acquisitions at ultrahigh magnetic fields should enable the acquisition of high quality spectra.

In this work, we present the first systematic ^{137}Ba SSNMR study of a series of barium-containing species using a combination of frequency-stepped NMR techniques and the WURST−QCPMG pulse sequence. The ^{137}Ba NMR spectra of six barium-containing compounds, including barium nitrate, barium carbonate, barium chlorate monohydrate, barium chloride, barium chloride dihydrate, and barium hydrogen phosphate, have been acquired at two different field strengths (9.4 and 21.1 T), and anisotropic quadrupolar and chemical shift tensor parameters obtained via spectral analysis are presented. In addition, experimental data are complemented by a series of theoretical ^{137}Ba EFG tensors, calculated using plane-wave CASTEP methods,[40] in order to draw correlations between the experimental NMR parameters, the calculated NMR tensors, and the local Ba environments.

Experimental Details

Samples of barium nitrate ($Ba(NO_3)_2$), barium carbonate ($BaCO_3$), barium chlorate monohydrate ($Ba(ClO_3)_2 \cdot H_2O$), barium chloride dihydrate ($BaCl_2 \cdot 2H_2O$), anhydrous barium chloride ($BaCl_2$), and barium hydrogen phosphate ($BaHPO_4$) were purchased from Sigma-Aldrich, and their identities were confirmed using powder X-ray diffraction (XRD) (Supporting Information, Figures S1−S6). Powder X-ray diffraction data were collected on a Bruker Apex 2 Kappa diffractometer at room temperature, using graphite monochromatized Mo Kα radiation ($\lambda = 0.71073$ Å).

Solid-State NMR. ^{137}Ba SSNMR experiments were performed on a Varian Infinity Plus spectrometer at the University of Windsor equipped with a 9.4 T ($\nu_0(^1H) = 399.73$ MHz) Oxford wide-bore magnet ($\nu_0(^{137}Ba) = 44.422$ MHz) and a 21.1 T ($\nu_0(^1H) = 900.08$ MHz) Bruker Avance II spectrometer ($\nu_0(^{137}Ba) = 100.02$ MHz) at the National Ultrahigh-Field NMR Facility for Solids in Ottawa, Canada. In most cases, the NMR powder patterns were much wider than the excitation bandwidth achievable with a standard high power rectangular pulse; hence, spectra were acquired by stepping the transmitter frequency across the entire central transition (CT) powder pattern in even increments, collecting the individual subspectra, and coadding them to form the total pattern[41,42] (see the Supporting Information, Tables S1 and S2, for full experimental details). Barium chemical shifts were referenced to a 1 M aqueous solution of $BaCl_2$ ($\delta_{iso} = 0.0$ ppm).[32] Analytical simulations of ^{137}Ba NMR spectra were performed using WSolids.[43] The uncertainties in the NMR tensor parameters were determined by visual comparison of the experimental and simulated spectra, and bidirectional variation of single parameters from their values corresponding to the best fit.

Experiments at 9.4 T. Samples were finely ground and packed into either 5 mm o.d. zirconium oxide MAS rotors or 5 mm glass NMR tubes. ^{137}Ba NMR spectra were acquired using either a Varian 5 mm double-resonance (HX) static probe or a Varian 5 mm triple-resonance (HXY) MAS probe. All spectra were collected using the WURST−QCPMG pulse sequence.[35,37] WURST-80 pulse shapes[44] were used with a 50 μs WURST pulse length, and swept at a rate of 10 or 40 MHz/ms with an offset of either 250 or 1000 kHz and an rf power of 28 kHz. The number of echoes ranged between 40 and 160, depending on the transverse relaxation characteristics of ^{137}Ba in each sample. A spectral width of either 500 or 800 kHz and an optimized recycle delay of 0.1 s were used. The frequency step size was set between 100 and 200 kHz, in order to ensure uniform excitation. Further experimental details are given in Table S1 of the Supporting Information. High-power proton decoupling was tested for all proton-containing samples ($\nu(^1H) = 35$ kHz); the only differences were observed for barium chloride dihydrate (vide infra).

Experiments at 21.1 T. Samples were ground and packed into 7 mm o.d. zirconium oxide rotors. ^{137}Ba NMR spectra were acquired with a 7 mm static probe using the frequency-stepped techniques outlined above, with a solid-echo pulse sequence of the form $(\pi/2)_x$-τ_1-$(\pi/2)_y$-τ_2-acq, where τ_1 and τ_2 represent interpulse delays. Experiments were conducted with a selective $\pi/2$ pulse width of 4 μs ($\nu_1 = 31$ kHz), spectral widths between 250 kHz and 1 MHz, calibrated recycle delays between 0.2 and 0.5 s, and transmitter frequency offsets of 100 kHz. Further experimental details are given in Table S2 of the Supporting Information. In the case of the barium hydrogen phosphate sample, the ^{137}Ba NMR spectrum was collected using the WURST−QCPMG pulse sequence.[35,37] WURST-80 pulse shapes[44] with a 50 μs WURST pulse length, swept at a rate of 20 MHz/ms, a sweep width of 1000 kHz, and rf power of 6 kHz were used. The number of echoes was set to 96. A spectral width of 1000 kHz and recycle delay of 0.2 s were used.

Computational Methods. ^{137}Ba EFG and CS tensor parameters were calculated for all structures. Ab initio plane-wave density functional theory (DFT) calculations were performed using the CASTEP NMR program[40,45] in the Materials Studio 4.3 environment on a HP xw4400 workstation with a single Intel Dual-Core 2.67 GHz processor and 8 GB DDR RAM. Ultrasoft pseudopotentials were used for ^{137}Ba EFG calculations

TABLE 1: Summary of the Experimental ^{137}Ba NMR Parameters

	$\lvert C_Q(^{137}Ba)\rvert^a$/MHz	$\eta_Q{}^b$	$\delta_{iso}{}^c$/ppm	Ω^d/ppm	κ^e	α^f/deg	β/deg	γ/deg
$Ba(NO_3)_2$	7.0(1)	0.01(1)	−42(8)	25(20)	0.8(2)	40(20)	10(25)	
$BaCO_3$	17.4(6)	0.33(4)	50(200)	150(150)	0.5(5)			
$Ba(ClO_3)_2 \cdot H_2O$	25.4(6)	0.48(4)	0(200)	200(100)	−0.8(2)			
$BaCl_2 \cdot 2H_2O$	28.8(3)	0.94(2)	150(100)	150(150)	−0.5(5)			
$BaCl_2$	28.7(3)	0.81(2)	200(200)	400(300)	0.5(5)			
$BaHPO_4$, site 1	15.5(1.0)	0.85(4)	−120(60)					
$BaHPO_4$, site 2	22.5(1.0)	0.82(4)	0(200)					

[a] $C_Q = eQV_{33}/h$. [b] $\eta_Q = (V_{11} - V_{22})/V_{33}$. [c] $\delta_{iso} = (\delta_{11} + \delta_{22} + \delta_{33})/3$. [d] $\Omega = \delta_{11} - \delta_{33}$. [e] $\kappa = 3(\delta_{22} - \delta_{iso})/\Omega$. [f] Conventions for the Euler angles are described in the WSolids software package.[36]

with a plane wave basis set cutoff of 550 eV in a fine accuracy basis set with Monkhorst−Pack k-space grid sizes of 4 × 4 × 4, 5 × 3 × 4, 3 × 3 × 3, 4 × 2 × 4, 3 × 3 × 5, and 4 × 1 × 1 for barium nitrate, barium carbonate, barium chlorate monohydrate, barium chloride dihydrate, anhydrous barium chloride, and barium hydrogen phosphate, respectively. The Perdew, Burke, and Ernzerhof (PBE) functionals were used in the generalized gradient approximation (GGA) for the exchange-correlation energy.[46,47] The magnetic shielding tensors for ^{137}Ba were calculated in a fine accuracy basis set using the projector augmented-wave method (GIPAW) implemented in the CASTEP code.[48,49] Relativistic effects are included in CASTEP calculations at the level of the scalar-relativistic zeroth-order regular approximation (ZORA).[50] The chemical shifts were calculated using $\delta_{iso}(sample) - \delta_{iso}(ref) = \sigma_{iso}(ref) - \sigma_{iso}(sample)$, where $\delta_{iso}(ref)$ and $\sigma_{iso}(ref)$ are the ^{137}Ba experimental chemical shift (279 ppm)[32] and the calculated chemical shielding (5262.28 ppm) of $BaZrO_3$, respectively. The CIF crystal structure files used in the calculations were obtained from the literature.[51−58] Proton positions were geometry optimized only in the case of barium hydrogen phosphate, since the structures utilized in the calculations for barium chloride dihydrate and barium chlorate monohydrate were determined from neutron diffraction experiments.[56]

Results and Discussion

Solid-State ^{137}Ba NMR. In this section, we discuss the ^{137}Ba SSNMR data for a series of systems in which the Ba atoms are in distinct coordination environments. The NMR spectra were acquired at two different magnetic field strengths to enable accurate deconvolution of the contributions of the second-order quadrupolar interaction and the barium chemical shift anisotropy (CSA). The experimentally measured C_Q's range from 7.0 to 28.8 MHz (Table 1), with central transition powder pattern breadths ranging from 145 kHz to 4.0 MHz at 9.4 T.

Barium Nitrate. Using the WURST−QCPMG pulse sequence,[37] the NMR pattern of barium nitrate was acquired very rapidly in a single experiment (11 min at 9.4 T with a breadth of 145 kHz, Figure 1). Analytical simulation of the spectrum reveals a single barium site, which is consistent with the known crystal structures.[51,52,58] The C_Q is 7.0 MHz, in agreement with that measured by Weiden and Weiss from a ^{137}Ba single-crystal NMR experiment.[59] This value is the smallest among the samples discussed herein (Table 1), likely due to the high spherical symmetry around the barium atom resulting from coordination to the 12 oxygen atoms of the nitrate groups arranged in a distorted cuboctahedron (Scheme 1a).[52,58] The η_Q is 0, indicating the axially symmetric electronic environment at the barium site (the V_{33} component of the EFG tensor is the unique component and is therefore positioned along the 3-fold rotational axis of the molecule). This agrees with the earlier assumptions of Weiden and Weiss, who assigned (but did not measure) an η_Q of 0 due to the molecular symmetry. The high field spectrum allows for the measurement of the barium CSA parameters (Figures 1 and S7, Supporting Information); however, the span (Ω) of the CS tensor is rather small, and represents a contribution of only 4% of the total breadth of the CT pattern. This indicates that accurate measurement of barium CS tensor parameters will be more challenging for complexes with larger values of C_Q, where the CT patterns are dominated by second-order quadrupolar contributions.

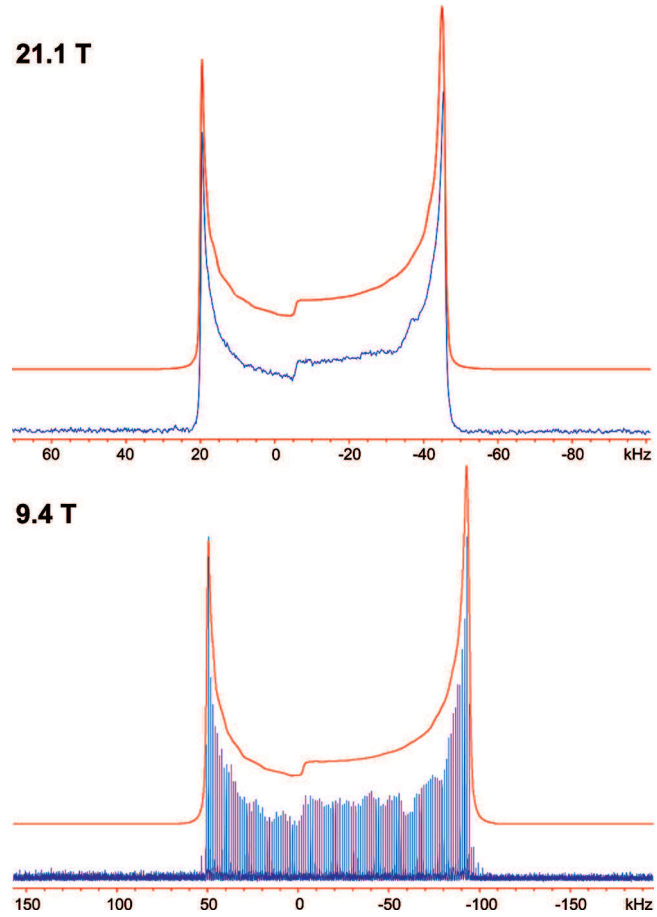

Figure 1. ^{137}Ba static SSNMR spectra of barium nitrate at two different magnetic field strengths.

Barium Carbonate. A static ^{137}Ba SSNMR spectrum of barium carbonate was previously obtained by Bastow, who reported an extremely long acquisition time (21 days at 9.4 T using the stepwise echo technique),[60] in spite of the large sample size that was used (i.e., in a 10 mm transverse coil). Our spectrum was obtained by collecting 15 and 7 subspectra at 9.4 and 21.1 T, respectively (the total experimental times were only 6.8 and 2.4 h for the whole patterns at 9.4 and 21.1 T, Figure 2). Simulations of both high- and low-field spectra reveal NMR

SCHEME 1: Coordination Environments of the Barium Atoms in (a) Barium Nitrate, (b) Barium Carbonate, (c) Barium Chlorate Monohydrate, (d) Barium Chloride Dihydrate, (e) Anhydrous Barium Chloride, (f) Barium Hydrogen Phosphate, Site 1, and (g) Barium Hydrogen Phosphate, Site 2

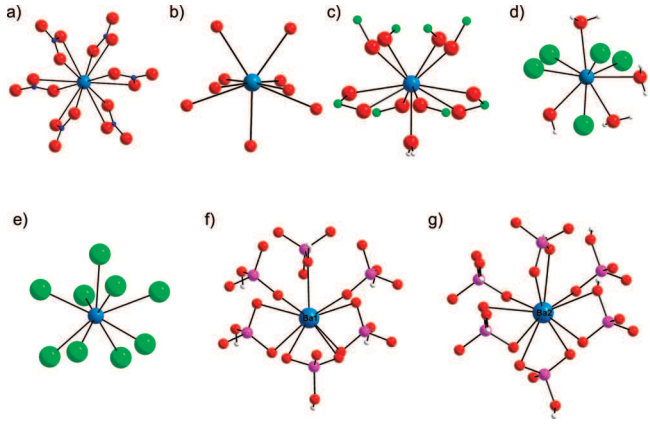

parameters identical to those obtained by Bastow. The C_Q is much larger than that of the nitrate sample, since the nine coordinating oxygen atoms (Scheme 1b) are positioned such that there is great variation in the Ba−O distances, and give rise to a nonspherically symmetric environment about the Ba center.[53] In addition, the Ba−O distances are shorter in the carbonate than in the nitrate, which may also augment the magnitude of C_Q. The value of η_Q indicates that V_{33} is the distinct component of the EFG tensor and should be oriented either along/within or perpendicular to a molecular symmetry element (there is a single mirror plane in this unit, which must also contain one of V_{11} or V_{22}). The slightly different values of V_{11} and V_{22} (and nonzero η_Q) correspond to the absence of a 3-fold (or higher) rotational symmetry axis. The barium CSA contribution is very small and its effect on the NMR spectra at both fields is negligible. This is confirmed by the ratio of the CT pattern breadths at 9.4 and 21.1 T, which is ca. 2.1:1.0; since the CT pattern breadths scale as the inverse of the external magnetic field, it is clear that the second order quadrupolar interaction is dominant. It is also interesting to note that the shapes of the CT powder patterns indicate some degree of disorder in the sample (the same phenomenon is observed in the spectrum reported by Bastow), since they do not have the typical sharp discontinuities associated with highly crystalline samples. This is not surprising, since carbonates are known to readily absorb water from the air. The presence of water in the sample was confirmed via ^{1}H MAS NMR experiments (Figures S8 and S9, Supporting Information).

Barium Chlorate Monohydrate. The ^{137}Ba quadrupolar parameters of barium chlorate monohydrate were obtained by Nakamura and Enokiya from the Zeeman splittings of ^{135}Ba and ^{137}Ba nuclei in a single crystal by using the proton signal enhancement caused by the frequency crossing of ν_{NQR}(^{135}Ba or ^{137}Ba) with ν_0(^{1}H); a directly excited NQR signal was not observed.[61] The low natural abundances of $^{135/137}$Ba make these types of NQR experiments challenging, and as a result, large sample sizes (i.e., on the order of 5−30 g) are traditionally utilized,[61,62] rendering these experiments impractical for cases in which sample sizes are limited.

We were able to obtain the ^{137}Ba SSNMR spectra at two different magnetic fields. The spectrum acquired at 9.4 T shows overlap between ^{137}Ba and ^{35}Cl/^{37}Cl powder patterns (ν_0($^{35/37}$Cl) = 39.260 and 32.680 MHz, Figure 3). The ^{35}Cl EFG parameters

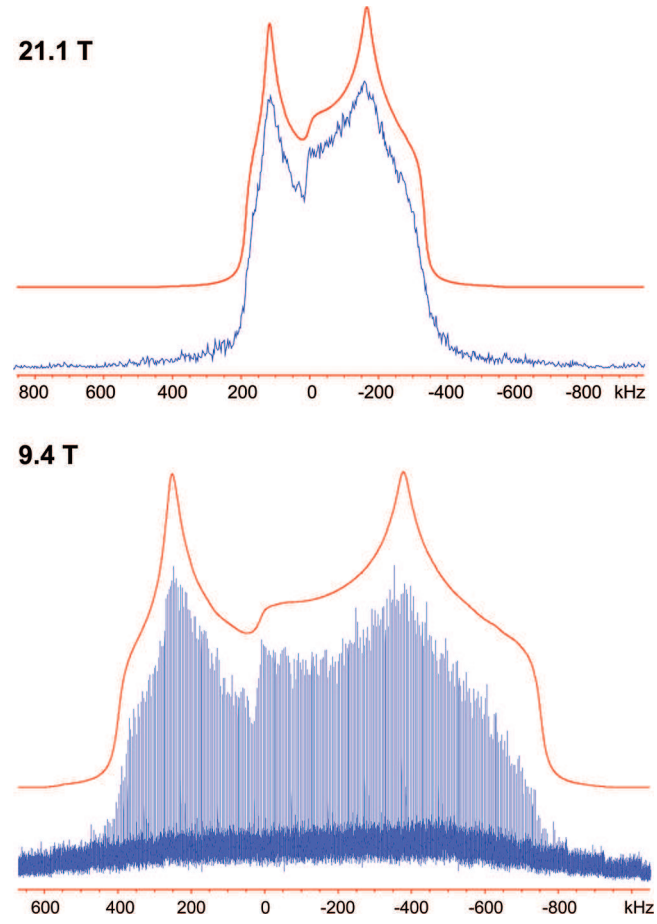

Figure 2. ^{137}Ba static SSNMR spectra of barium carbonate at two different magnetic field strengths.

were previously measured by NQR spectroscopy (C_Q = 58.687 MHz and η_Q = 0.027).[63−65] Using these parameters, analytical simulations reveal that the ^{35}Cl and ^{37}Cl NMR pattern breadths exceed 30 MHz, and result in the observed overlap; unfortunately, it is very difficult to obtain a precise fit of the overlapping patterns (Figure S10, Supporting Information). Due to the much higher natural abundance of chlorine (n.a. = 75.5 and 24.5% for ^{35}Cl and ^{37}Cl, respectively), as well as the difference in T_2 characteristics between ^{137}Ba and $^{35/37}$Cl, the ^{137}Ba signal in the low frequency side of the pattern is obstructed by the $^{35/37}$Cl signals. However, the ^{137}Ba NMR spectrum acquired at 21.1 T displays no such overlap, since the ^{137}Ba and ^{35}Cl Larmor frequencies are further apart ν_0($^{35/37}$Cl) = 88.125 and 73.356 MHz, and the CT pattern breadths scale as the inverse of B_0 (though traces of interference from the ^{137}Ba satellite transitions are observed). The barium ion in this site is surrounded by 1 water oxygen and 10 other oxygen atoms from different chlorate groups.[54] The larger C_Q compared to that of the previous two samples is due to further reduction of spherical symmetry at the barium site. The shortest Ba−O bond of 2.731 Å is to the lone water molecule in the arrangement of 11 oxygen atoms (the other 10 Ba−O distances range from 2.790 to 3.004 Å). η_Q = 0.48 indicates that V_{33} is the distinct component of the EFG tensor, which is likely oriented along the 2-fold rotational axis of the molecule, which includes the lone Ba−OH_2 bond (Scheme 1c).[54]

Dihydrate and Anhydrous Forms of Barium Chloride. The ^{137}Ba quadrupolar parameters of barium chloride dihydrate were previously obtained from NQR experiments on single crystal[66] and polycrystalline samples.[67] In the former case, the extraction

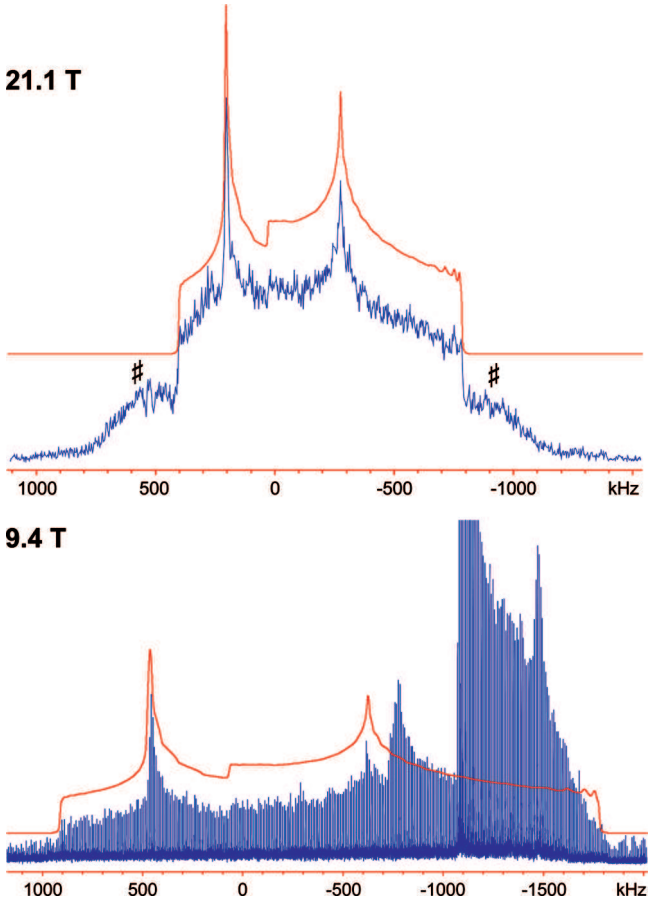

Figure 3. ^{137}Ba static SSNMR spectra of barium chlorate monohydrate at two different magnetic field strengths. Overlap between the ^{35}Cl CT and ^{37}Cl satellite transition (ST) with the ^{137}Ba spectrum is observed at 9.4 T. # denotes portions of the ^{137}Ba STs. The small distortions in the right-most "shoulders" of each simulated spectrum are artifacts arising from a limited number of angles in the total powder average.

of the quadrupolar parameters was complicated by crystal twinning, while, in the latter case, a very large amount of crystalline sample was used (i.e., 25 g) in order to obtain the signal (again, this can be inconvenient and impractical in many situations where sample sizes are limited). In contrast, our ^{137}Ba SSNMR spectra were obtained at 9.4 and 21.1 T using a small amount of a powdered sample (i.e., 0.2 g). Simulations of the spectra (Figure 4) reveal a single barium site, in agreement with the crystal structure.[56] The C_Q value is similar to that obtained from NQR; however, the η_Q value of 0.78(14) is different.[66,67] The η_Q value obtained from our NMR experiments is likely more accurate, since the previously reported η_Q value was estimated from calculations and quadrupolar parameters of analogous systems, and not directly measured in the NQR experiments (NQR experiments on spin-3/2 nuclei do not readily permit determination of η_Q,[68] unless special techniques are applied).[69,70] The barium atom is coordinated to four oxygen and five chlorine atoms (Scheme 1d), with Ba−O bond distances varying from 2.844 to 2.887 Å and Ba−Cl distances varying from 3.131 to 3.340 Å.[56] The chlorine and oxygen atoms are arranged such that no simple geometrical assignments of shape can be made; in fact, the arrangement of atoms has been described "approximately as a square antiprism with one square face enlarged to accommodate the fifth Cl^- ion".[56] The complete absence of spherical/platonic symmetry coupled with the different Ba−O and Ba−Cl distances and distinct electronic characteristics of the Cl and O atoms give rise to the largest C_Q observed in this series. Since η_Q is close to 1.0, it is known that V_{11} is the distinct component and V_{22} and V_{33} are very similar in magnitude. However, due to the absence of any symmetry elements, it is difficult to make any postulations regarding the orientation of the EFG tensor components.

The ^{137}Ba SSNMR spectra of the anhydrous form at both fields (Figure 4) indicate a single barium site, consistent with the crystal structure.[55] Simulations of these spectra reveal NMR parameters similar to those of the dihydrate sample. The barium atom in this case has a 9-fold coordination to chlorine atoms forming three-face centred trigonal prism (Scheme 1e), and the Ba−Cl bond distances vary from 3.063 to 3.544 Å.[55] Due to the difference between the barium chemical environments in the anhydrous and dihydrate samples and the much larger Ba−Cl distances in the former, it is difficult to qualitatively rationalize the similarity of the C_Q values (though, certainly, the aspherical environment yields a large C_Q). Again, the η_Q value of the anhydrous form indicates that V_{11} is the distinct component; however, in this case, V_{11} must be oriented perpendicular to the mirror plane, since $V_{22} \approx V_{33}$.

It would be very difficult to differentiate the Ba sites in the anhydrous and dihydrate forms based on the values of C_Q and η_Q alone. However, there is a large difference in their transverse relaxation times, $T_2(^{137}\text{Ba})$, which are measured from the QCPMG echo trains. T_2 is much longer in the anhydrous form (13.2 ± 5.2 ms) than in the dihydrate (3.1 ± 2.0 ms). This difference arises from the presence of dipolar couplings between water protons and ^{137}Ba nuclei in the dihydrate sample, which serve to increase the efficiency of transverse relaxation; this was confirmed by applying ^{1}H decoupling during acquisition, which helps to reduce the dipolar contribution to the overall transverse relaxation (T_2 = 9.6 ± 5.7 ms). In principle, one could differentiate these sites in a mixed sample by acquiring QCPMG echo trains of varying lengths.

Barium Hydrogen Phosphate. The acquisitions of the ^{137}Ba SSNMR spectra of barium hydrogen phosphate were more challenging than those of the previous systems, due to the presence of two overlapping powder patterns (Figure 5) resulting from two crystallographically distinct barium sites, as well as substantially reduced transverse relaxation times (and correspondingly shorter CPMG trains). We were unable to obtain a full, high S/N powder pattern at 9.4 T; however, a high quality spectrum was acquired at 21.1 T using the WURST−QCPMG pulse sequence. The two sites have very different NMR parameters which reflect the difference in their coordination environments[57] and demonstrate the sensitivity of the ^{137}Ba NMR to the structural differences. The two barium sites are 9-fold (Ba1) and 10-fold (Ba2) (Scheme 1f,g) coordinated by oxygen atoms, and are assigned to the smaller and larger C_Q values, respectively, on the basis of the higher spherical symmetry of the former (see the computational section below for further discussion). The high η_Q values indicate V_{11} is the distinct component of the EFG tensor in both cases (vide infra).

Theoretical Calculations of ^{137}Ba EFG and CS Tensors. Ab initio calculations were performed in order to correlate the ^{137}Ba EFG tensors to the solid-state structure at the barium sites. The development of such correlations is crucial for future applications of ^{137}Ba SSNMR spectroscopy and associated structural interpretations for many barium-containing systems which are disordered or do not have known crystal structures. Due to the periodic nature of the systems herein, CASTEP software was used for the calculations of the NMR parameters (see Computational Methods for details). The results of all of these calculations are compared to the experimental values in

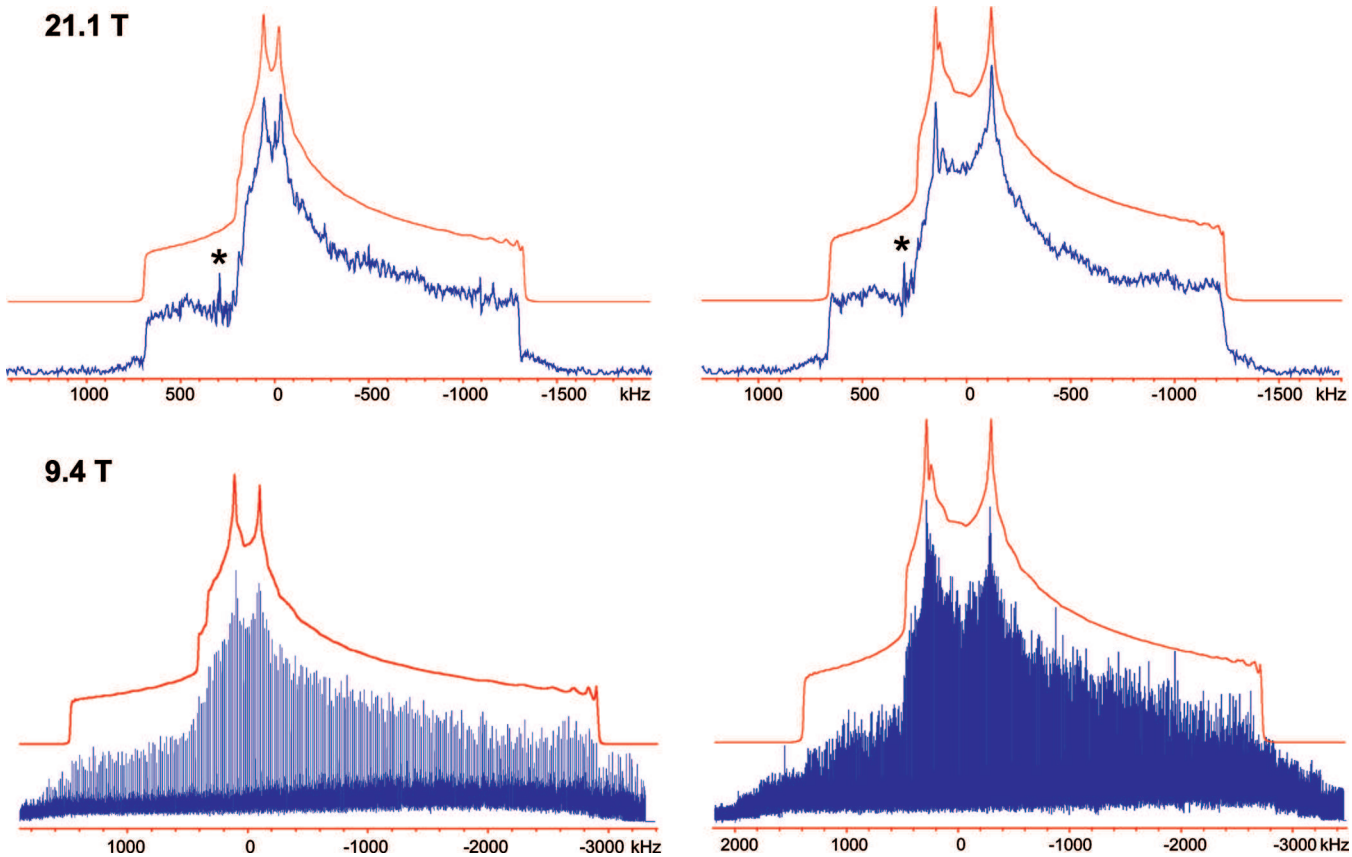

Figure 4. ^{137}Ba static SSNMR spectra of barium chloride dihydrate (left) and anhydrous barium chloride (right) at two different magnetic field strengths. ∗ indicates interferences from an FM radio frequency.

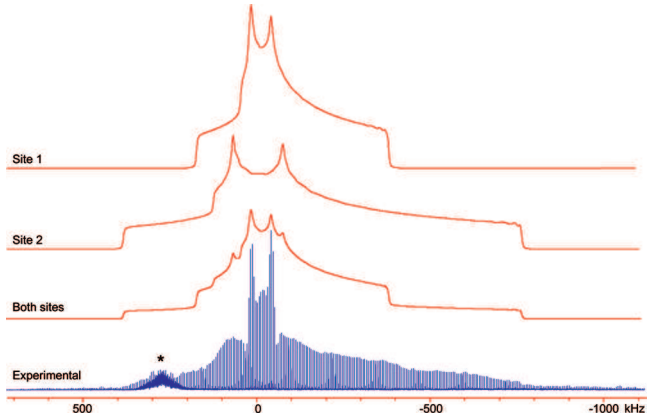

Figure 5. ^{137}Ba static SSNMR spectrum of barium hydrogen phosphate and its simulation at 21.1 T. ∗ indicates interferences from an FM radio frequency.

Tables 2 and S3 (Supporting Information). Plotting the experimental C_Q's versus the calculated values provides an excellent linear correlation (Figure 6a); however, this correlation is only satisfactory for the η_Q values (see Figure 6b and discussion below). Since the anisotropic chemical shift parameters have a minimal influence on the ^{137}Ba CT NMR spectra, it is difficult to make accurate comparisons of these data and the theoretically calculated magnetic shielding tensors; hence, the barium CS tensor parameters are not discussed in detail herein (some preliminary data is summarized in Table S3 of the Supporting Information).

CASTEP calculations were performed on the three different structures of barium nitrate reported in the literature.[51,52,58] The best agreement with experiment is obtained from calculations utilizing coordinates based on the most recently reported structure by Trounov et al. (Tables 2 and S4, Supporting Information). While all calculations predict axially symmetric EFG tensors ($\eta_Q = 0$), theoretically calculated values of C_Q vary with subtle changes in molecular structure, demonstrating that even small displacements in O positions can lead to significant changes in the magnitude of V_{33}. Furthermore, geometry optimization of the structure and the use of varying degrees of basis set flexibility in the EFG calculations did not result in significant variation in the calculated values of C_Q (Table S4, Supporting Information). It is likely that limitations in the basis set or density functional may account for discrepancies between experimental and calculated C_Q values, and not long-range electrostatic interactions, since these are inherently taken into account in the CASTEP calculations. The largest component of the EFG tensor, V_{33}, is aligned along the 3-fold rotational axis of the molecule, in accordance with the axial symmetry of the EFG tensor (Figure 7a), and consistent with our predictions based on symmetry.

The calculated C_Q for barium carbonate is in good agreement with the experimental value. V_{33}, the distinct component of the EFG tensor, is positioned within the crystallographic mirror plane (Figure 7b), and lies close to an approximate plane formed by four O atoms. The theoretical value of η_Q is 0.06, which indicates that the EFG tensor is essentially axially symmetric ($V_{11} \approx V_{22}$), and that V_{11} and V_{22} are directed into similar chemical environments. This is surprisingly different from the experimentally measured tensor, in which V_{11} and V_{22} are not similar. We are uncertain of the origin of this discrepancy; however, given the mirror plane symmetry of the BaO_9 coordination environment, and the distinct V_{11} and V_{22} environ-

TABLE 2: Comparison of the Experimental and CASTEP-Calculated ^{137}Ba EFG Tensor Parameters

	V_{11} (au)	V_{22} (au)	V_{33} (au)	$C_Q(^{137}Ba)^a$/MHz	η_Q
$Ba(NO_3)_2$ Exp.				7.0(1)	0.01(1)
$Ba(NO_3)_2$ Cal.	0.0464	0.0464	−0.0927	−5.3	0.00
$BaCO_3$ Exp.				17.4(6)	0.33(4)
$BaCO_3$ Cal.	−0.1241	−0.1385	0.2626	15.1	0.06
$Ba(ClO_3)_2 \cdot H_2O$ Exp.				25.4(6)	0.48(4)
$Ba(ClO_3)_2 \cdot H_2O$ Cal.	0.0629	0.3868	−0.4497	−25.9	0.72
$BaCl_2 \cdot 2H_2O$ Exp.				28.8(3)	0.94(2)
$BaCl_2 \cdot 2H_2O$ Cal.	0.0077	0.5490	−0.5567	−32.0	0.97
$BaCl_2$ Exp.				28.7(3)	0.81(2)
$BaCl_2$ Cal.	0.0301	0.4688	−0.4989	−28.7	0.88
$BaHPO_4$, site 1 Exp.				15.5(1.0)	0.85(4)
$BaHPO_4$, site 1 Cal.	0.0123	0.2625	−0.2748	−15.8	0.91
$BaHPO_4$, site 2 Exp.				22.5(1.0)	0.82(4)
$BaHPO_4$, site 2 Cal.	0.0882	0.3411	−0.4293	−24.7	0.59

[a] The signs of experimental C_Q values are unknown; the signs of theoretically calculated values of C_Q are determined from calculations.

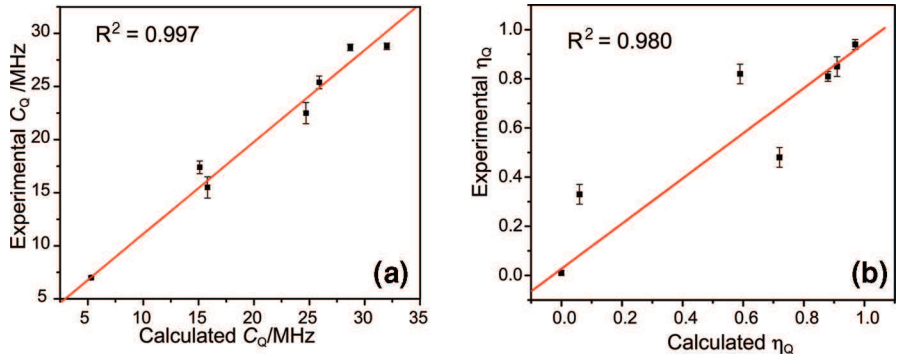

Figure 6. Correlations between the experimental and calculated ^{137}Ba (a) C_Q and (b) η_Q values.

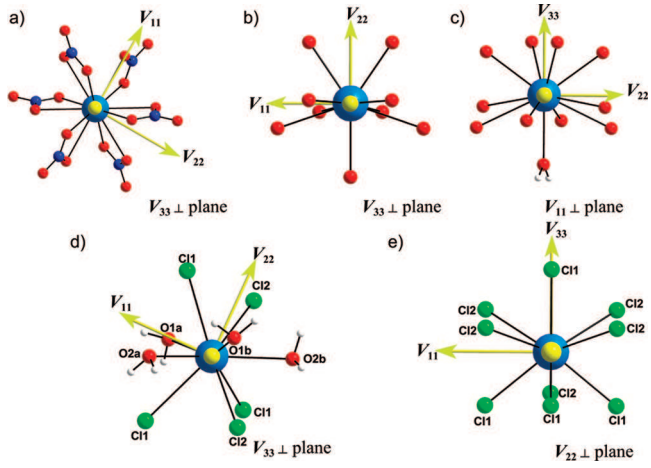

Figure 7. Theoretically calculated ^{137}Ba EFG tensor orientations in (a) barium nitrate, (b) barium carbonate, (c) barium chlorate monohydrate, (d) barium chloride dihydrate, and (e) anhydrous barium chloride.

ments indicated by symmetry and by calculated tensor orientations, we believe that the experimental value is far more reliable.

The calculated C_Q value in the barium chlorate monohydrate case is in excellent agreement with experiment; however, the calculated η_Q is slightly higher. In this case, the discrepancy between the experimental and theoretical η_Q values may result from the observation of an "average" or "effective" η_Q, which results from librational motion of the water molecules[54] which may alter the magnitude(s) of V_{11} and/or V_{22}. As expected, the largest component of the EFG, V_{33}, is oriented along the Ba−O_{water} bond ($\angle V_{33}$−Ba−O = 180°), which lies along the C_2 rotational axis, with V_{11} and V_{22} oriented in different environments (Figure 7c).

Both the C_Q and η_Q values for barium chloride dihydrate are in good agreement with experiment. As discussed above, these large values of C_Q result from the absence of any sort of spherical/platonic symmetry about the barium center. In this case, V_{11} is the distinct component of the EFG tensor, and is oriented almost in the center of a distorted pyramid formed by two Cl1, O1a, and O2a atoms, and V_{22} is oriented at an angle with the plane formed by O1a, O2a, and O2b ($\angle V_{22}$−Ba−O2b = 67.36°, Figure 7d). For the anhydrous system, both the C_Q and η_Q values are in excellent agreement with experimental data. Again, V_{11} is the distinct component, and as predicted is oriented perpendicular to a crystallographic mirror plane formed by one Cl2 and two Cl1 atoms, and bisects two separate planes formed by one Cl1 and two Cl2 atoms (Figure 7e). V_{22} and V_{33} are contained within the former plane, with the latter oriented very close (ca. 14°) to the shorter in-plane Ba−Cl2 bond. These two systems have very similar local barium geometries in terms of atom positions, as evidenced by the similar values of C_Q and tensor orientations; however, the disparate η_Q values reflect the changing atom identities (O vs Cl) and bond lengths.

The calculated values of C_Q and η_Q for barium hydrogen phosphate are in very good agreement with experiment and confirm the assignment of the two sites based on the NMR data. The nine-coordinate Ba1 site has a crystallographic mirror plane which contains the lone Ba−O−H arrangement of atoms; the O atoms are arranged in a distorted monocapped square prismatic environment. V_{11} is the distinct component, and is directed perpendicular to this plane; V_{22} and V_{33} are positioned within the plane, oriented at ca. 11 and 101°, respectively, from the unique Ba−O(H) bond (Figure 8a). The Ba2 site is in a general position with no symmetry elements, and much lower spherical symmetry than Ba1. V_{11} is again the distinct component, and is oriented along the direction of the two bidentate-

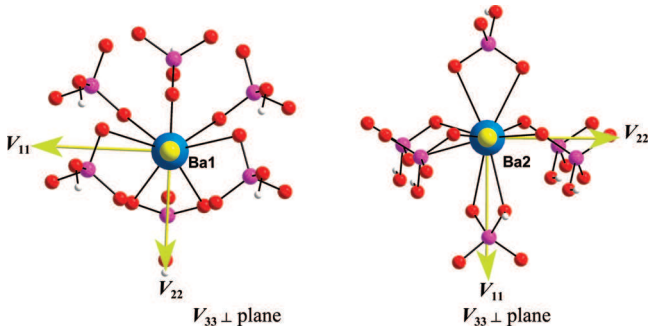

Figure 8. Theoretically calculated ^{137}Ba EFG tensor orientations in $BaHPO_4$.

bound phosphate groups, Figure 8b (i.e., $V_{11}-Ba-P_{bident}$ of 1.4 and 7.9°). V_{22} and V_{33} are directed into similar environments comprised of a shallow pyramid of O atoms from four monodentate phosphate ligands (one of them is nominally bidentate with a much lengthier Ba−O bond, V_{22} lies ca. 6.7° from this bond).

Conclusions

Herein, we have shown that acquisition of ^{137}Ba ultrawideline SSNMR spectra of barium-containing materials is feasible at moderate and ultrahigh magnetic field strengths. Using the WURST−QCPMG pulse sequence, along with frequency-stepped acquisitions, the ^{137}Ba NMR spectra can be rapidly acquired with high resolution and reasonably good S/N. Furthermore, using ultrahigh magnetic field strengths, experimental times can be significantly decreased (or S/N enhanced) due to the reduction in the second-order quadrupolar pattern breadths resulting from their inverse dependence on the external magnetic field strength.

The shapes and breadths of the ^{137}Ba NMR patterns are dominated by the quadrupolar interaction. The quadrupolar parameters, C_Q and η_Q, which are extracted from these spectra are extremely sensitive to the nature of the barium site geometries, symmetries, and coordination environments. The values of C_Q increase in magnitude as the Ba environments become less spherically symmetric. Theoretical calculations of the ^{137}Ba EFG tensor parameters are generally in good agreement with the experimental values, and will undoubtedly be helpful in future structural predictions for which crystallographic data are not available. Further, the ^{137}Ba EFG tensor orientations provide insight into the origin of these tensors and their correlations to molecular structure and symmetry. From this work, we hope that ^{137}Ba SSNMR spectroscopy will continue to be applied to characterize molecular structure (and potentially dynamics) in a wide variety of barium-containing systems, aiding chemists and material scientists in understanding these systems at the molecular level.

Acknowledgment. R.W.S. thanks the Natural Sciences and Engineering Research Council of Canada (NSERC) for supporting this research. R.W.S. also acknowledges the Ontario Ministry of Research and Innovation for support in the form of an Early Researcher Award. We thank the Canada Foundation for Innovation (CFI), the Ontario Innovation Trust (OIT), the University of Windsor, and NSERC for funding of the solid-state NMR centre at the University of Windsor, and the Centre for Catalysis and Materials Research (CCMR) at Windsor for additional support. H.H. thanks the Ministry of Training, Colleges and Universities for an Ontario Graduate Scholarship and UW for a Tuition Scholarship. Dr. Victor Terskikh, Dr. Luke O'Dell, and Mr. Aaron Rossini are thanked for helpful comments. Access to the 900 MHz NMR spectrometer and CASTEP software was provided by the National Ultrahigh-Field NMR Facility for Solids (Ottawa, Canada), a national research facility funded by CFI, OIT, Recherche Québec, the National Research Council Canada, and Bruker BioSpin and managed by the University of Ottawa (www.nmr900.ca). NSERC is acknowledged for a Major Resources Support grant.

Supporting Information Available: Additional experimental details and powder XRD data. This material is available free of charge via the Internet at http://pubs.acs.org.

References and Notes

(1) Siegel, R.; Nakashima, T. T.; Wasylishen, R. E. *Concepts Magn. Reson., Part A* **2005**, *26A*, 47–61.
(2) Ashbrook, S. E.; Duer, M. J. *Concepts Magn. Reson., Part A* **2006**, *28A*, 183–248.
(3) Smith, M. E.; Van Eck, E. R. H. *Prog. Nucl. Magn. Reson. Spectrosc.* **1999**, *34*, 159–201.
(4) Ashbrook, S. E. *Phys. Chem. Chem. Phys.* **2009**, *11*, 6892–6905.
(5) Chapman, R. P.; Widdifield, C. M.; Bryce, D. L. *Prog. Nucl. Magn. Reson. Spectrosc.* **2009**, *55*, 215–237.
(6) Hamaed, H.; Laschuk, M. W.; Terskikh, V. V.; Schurko, R. W. *J. Am. Chem. Soc.* **2009**, *131*, 8271–8279.
(7) Chen, F.; Ma, G.; Cavell, R. G.; Terskikh, V. V.; Wasylishen, R. E. *Chem. Commun.* **2008**, 5933–5935.
(8) Lipton, A. S.; Wright, T. A.; Bowman, M. K.; Reger, D. L.; Ellis, P. D. *J. Am. Chem. Soc.* **2002**, *124*, 5850–5860.
(9) Michaelis, V. K.; Aguiar, P. M.; Terskikh, V. V.; Kroeker, S. *Chem. Commun.* **2009**, 4660–4662.
(10) O'Dell, L. A.; Schurko, R. W. *Phys. Chem. Chem. Phys.* **2009**, *11*, 7069–7077.
(11) Jakobsen, H. J.; Bildsoe, H.; Skibsted, J.; Brorson, M.; Gor'kov, P.; Gan, Z. *J. Magn. Reson.* **2010**, *202*, 173–179.
(12) Moudrakovski, I.; Lang, S.; Patchkovskii, S.; Ripmeester, J. *J. Phys. Chem. A* **2010**, *114*, 309–316.
(13) Sutrisno, A.; Terskikh, V. V.; Huang, Y. *Chem. Commun.* **2009**, 186–188.
(14) Bowers, G. M.; Lipton, A. S.; Mueller, K. T. *Solid State Nucl. Magn. Reson.* **2006**, *29*, 95–103.
(15) Cahill, L. S.; Hanna, J. V.; Wong, A.; Freitas, J. C. C.; Yates, J. R.; Harris, R. K.; Smith, M. E. *Chem.—Eur. J.* **2009**, *15*, 9785–9798, S9785/9781−S9785/9783.
(16) Pallister, P. J.; Moudrakovski, I. L.; Ripmeester, J. A. *Phys. Chem. Chem. Phys.* **2009**, *11*, 11487–11500.
(17) Laurencin, D.; Wong, A.; Chrzanowski, W.; Knowles, J. C.; Qiu, D.; Pickup, D. M.; Newport, R. J.; Gan, Z.; Duer, M. J.; Smith, M. E. *Phys. Chem. Chem. Phys.* **2010**, *12*, 1081–1091.
(18) Laurencin, D.; Gervais, C.; Wong, A.; Coelho, C.; Mauri, F.; Massiot, D.; Smith, M. E.; Bonhomme, C. *J. Am. Chem. Soc.* **2009**, *131*, 13430–13440.
(19) Bryce, D. L.; Bultz, E. B.; Aebi, D. *J. Am. Chem. Soc.* **2008**, *130*, 9282–9292.
(20) Harris, R. K.; Becker, E. D.; Cabral De Menezes, S. M.; Goodfellow, R.; Granger, P. *Pure Appl. Chem.* **2001**, *73*, 1795–1818.
(21) Dibello, P. M.; Manganaro, J. L.; Aguinaldo, E. R.; Mahmood, T.; Lindahl, C. B. *Kirk-Othmer Encycl. Chem. Technol. (5th Ed.)* **2004**, *3*, 351–375.
(22) Vijatovic, M. M.; Bobic, J. D.; Stojanovic, B. D. *Sci. Sintering* **2008**, *40*, 235–244.
(23) Symalla, M. O.; Drochner, A.; Vogel, H.; Buechel, R.; Pratsinis, S. E.; Baiker, A. *Appl. Catal., B* **2009**, *89*, 41–48.
(24) Taye, A.; Klotzsche, G.; Michel, D.; Mulla-Osman, S.; Bottcher, R. *J. Phys.: Condens. Matter* **1999**, *11*, 871–879.
(25) Dec, S. F.; Davis, M. F.; Maciel, G. E.; Bronnimann, C. E.; Fitzgerald, J. J.; Han, S. S. *Inorg. Chem.* **1993**, *32*, 955–959.
(26) Bastow, T. J. *J. Phys.: Condens. Matter* **1989**, *1*, 4985–4991.
(27) Forbes, C. E.; Hammond, W. B.; Cipollini, N. E.; Lynch, J. F. *J. Chem. Soc., Chem. Commun.* **1987**, 433–436.
(28) Bastow, T. J.; Whitfield, H. J. *Solid State Commun.* **2001**, *117*, 483–488.
(29) Shore, J.; Yang, S.; Haase, J.; Schwartz, D.; Oldfield, E. *Phys. Rev. B: Condens. Matter* **1992**, *46*, 595–598.
(30) Yakubowskii, A.; Egorov, A.; Lutgemeier, H. *Appl. Magn. Reson.* **1992**, *3*, 665–676.
(31) Gervais, C.; Veautier, D.; Smith, M. E.; Babonneau, F.; Belleville, P.; Sanchez, C. *Solid State Nucl. Magn. Reson.* **2004**, *26*, 147–152.

(32) MacKenzie, K. J. D.; Meinhold, R. H. *Ceram. Int.* **2000**, *26*, 87–92.
(33) Sutrisno, A.; Lu, C.; Lipson, R. H.; Huang, Y. *J. Phys. Chem. C* **2009**, *113*, 21196–21201.
(34) Larsen, F. H.; Lipton, A. S.; Jakobsen, H. J.; Nielsen, N. C.; Ellis, P. D. *J. Am. Chem. Soc.* **1999**, *121*, 3783–3784.
(35) O'Dell, L. A.; Rossini, A. J.; Schurko, R. W. *Chem. Phys. Lett.* **2009**, *468*, 330–335.
(36) O'Dell, L. A.; Schurko, R. W. *J. Am. Chem. Soc.* **2009**, *131*, 6658–6659.
(37) O'Dell, L. A.; Schurko, R. W. *Chem. Phys. Lett.* **2008**, *464*, 97–102.
(38) Bowers, G. M.; Kirkpatrick, R. J. *J. Magn. Reson.* **2007**, *188*, 311–321.
(39) Bhattacharyya, R.; Frydman, L. *J. Chem. Phys.* **2007**, *127*, 194503/194501–194503/194508.
(40) Clark, S. J.; Segall, M. D.; Pickard, C. J.; Hasnip, P. J.; Probert, M. I. J.; Refson, K.; Payne, M. C. *Z. Kristallogr.* **2005**, *220*, 567–570.
(41) Medek, A.; Frydman, V.; Frydman, L. *J. Phys. Chem. A* **1999**, *103*, 4830–4835.
(42) Massiot, D.; Farnan, I.; Gautier, N.; Trumeau, D.; Trokiner, A.; Coutures, J. P. *Solid State Nucl. Magn. Reson.* **1995**, *4*, 241–248.
(43) Eichele, K.; Wasylishen, R. E. *WSolids NMR Simulation Package*, 1.17.30 ed.; Dalhousie University: Halifax, CA, 2001.
(44) Kupce, E.; Freeman, R. *J. Magn. Reson., Ser. A* **1995**, *115*, 273–276.
(45) Profeta, M.; Mauri, F.; Pickard, C. J. *J. Am. Chem. Soc.* **2003**, *125*, 541–548.
(46) Perdew, J. P.; Burke, K.; Ernzerhof, M. *Phys. Rev. Lett.* **1996**, *77*, 3865–3868.
(47) Perdew, J. P.; Burke, K.; Ernzerhof, M. *Phys. Rev. Lett.* **1998**, *80*, 891.
(48) Pickard, C. J.; Mauri, F. *Phys. Rev. B* **2001**, *63*, 245101/245101–245101/245113.
(49) Yates, J. R.; Pickard, C. J.; Mauri, F. *Phys. Rev. B* **2007**, *76*, 024401/024401–024401/024411.
(50) Yates, J. R.; Pickard, C. J.; Payne, M. C.; Mauri, F. *J. Chem. Phys.* **2003**, *118*, 5746–5753.
(51) Birnstock, R. *Z. Kristallogr., Kristallgeom., Kristallphys., Kristallchem.* **1967**, *124*, 310–334.
(52) Nowotny, H.; Heger, G. *Acta Crystallogr., Sect. C: Cryst. Struct. Commun.* **1983**, *C39*, 952–956.
(53) Antao, S. M.; Hassan, I. *Phys. Chem. Miner.* **2007**, *34*, 573–580.
(54) Sikka, S. K.; Momin, S. N.; Rajagopal, H.; Chidambaram, R. *J. Chem. Phys.* **1968**, *48*, 1883–1890.
(55) Busing, W. R. *Trans. Am. Crystallogr. Assoc.* **1970**, *6*, 57–72.
(56) Padmanabhan, V. M.; Busing, W. R.; Levy, H. A. *Acta Crystallogr., Sect. B: Struct. Sci.* **1978**, *B34*, 2290–2292.
(57) BenChaabane, T.; Smiri, L.; Bulou, A. *Solid State Sci.* **2004**, *6*, 197–204.
(58) Trounov, V. A.; Tserkovnaya, E. A.; Gurin, V. N.; Korsukova, M. M.; Derkachenko, L. I.; Nikanorov, S. P. *Tech. Phys. Lett.* **2002**, *28*, 351–353.
(59) Weiden, N.; Weiss, A. *Magn. Reson. Relat. Phenom., Proc. Congr. AMPERE, 18th* **1975**, *1*, 257–258.
(60) Bastow, T. J. *Chem. Phys. Lett.* **2002**, *354*, 156–159.
(61) Nakamura, S.; Enokiya, H. *J. Phys. Soc. Jpn.* **1963**, *18*, 183–188.
(62) Volkov, A. F. *J. Magn. Reson.* **1973**, *11*, 73–76.
(63) Krishnan, V.; Moorthy, T. V. K.; Ramakrishna, J. *Z. Naturforsch., A: Phys. Sci.* **1986**, *41A*, 338–340.
(64) Vargas, H.; Pelzl, J.; Dimitropoulos, C. *J. Magn. Reson.* **1978**, *30*, 423–429.
(65) Chihara, H.; Nakamura, N. *Landolt-Bornstein Group III: Condensed Matter; Volume 39: Nuclear Quadrupole Resonance Spectroscopy Data. Supplement to Volumes III/20 and III/31*; Springer: Berlin, Germany, 1998.
(66) Graybeal, J. D.; Pathania, M.; Ing, S. D. *J. Magn. Reson.* **1973**, *9*, 27–34.
(67) Graybeal, J. D.; McKown, R. J. *J. Phys. Chem.* **1969**, *73*, 3156–3157.
(68) Korneva, I.; Ostafin, M.; Sinyavsky, N.; Nogaj, B.; Mackowiak, M. *Solid State Nucl. Magn. Reson.* **2007**, *31*, 119–123.
(69) Harbison, G. S.; Slokenbergs, A. *Z. Naturforsch., A: Phys. Sci.* **1990**, *45*, 575–580.
(70) Harbison, G. S.; Slokenbergs, A.; Barbara, T. M. *J. Chem. Phys.* **1989**, *90*, 5292–5298.

JP102026M